LA-UR-01-0071
Approved for public release; distribution is unlimited.

Title: **Integrated System Simulation in X-ray Radiography**

Author(s): Thomas J. T. Kwan, Allen R. Mathews, Peggy J. Christenson, and Charles M. Snell

Submitted to:

http://lib-www.lanl.gov/la-pubs/00796143.pdf

Integrated System Simulation in X-ray Radiography

Thomas J. T. Kwan, Allen R. Mathews, Peggy J. Christenson, and Charles M. Snell

Los Alamos National Laboratory

Los Alamos, NM 87545 U.S.A.

Abstract

An integrated simulation capability is being developed to examine the fidelity of a dynamic radiographic system. This capability consists of a suite of simulation codes which individually model electromagnetic and particle transport phenomena and are chained together to model an entire radiographic event. Our study showed that the electron beam spot size at the converter target plays the key role in determining material edge locations. The angular spectrum is a relatively insensitive factor in radiographic fidelity. We also found that the full energy spectrum of the imaging photons must be modeled to obtain an accurate analysis of material densities.

Key words: radiography, plasma simulation, beam-plasma interaction,

PACS: 41.75.L, 52.65, 07.85.Y, 87.59.B

I. Introduction

In dynamic X-ray radiography, a pulsed, high-energy accelerator produces an intense beam of electrons that are focused onto a bremsstrahlung converter target. Interactions between the electrons and the converter target generate an X-ray pulse to image the internal structure of a dynamically evolving object. The resulting radiograph is then numerically analyzed using model fitting and tomographic reconstruction techniques to

determine material edges and density distribution. The process is schematically shown in Fig. 1. Accurate electron and photon transport models are needed to describe the radiation source and to analyze the resulting radiograph. The energy and angular spectra and the spot size of the photon source generated by the electron beam depend on electromagnetic and transport phenomena associated with the electron beam and the target. Furthermore, as the imaging photons traverse an object, they may be absorbed or scattered by the intervening material. Absorption leads to attenuation of the incident photon intensity, and scatter results in a non-uniform radiation background. In addition to the experimental object, shielding material, collimators, and other apparatus attenuate or scatter photons within the radiographic system. Finally, the detector adds a non-uniform background distribution. Each of these contributions must be taken into account to fully analyze data for the object.

An integrated system simulation capability, which consists of simulation codes for the various physical processes, has been developed to model the entire event. The Merlin electromagnetic particle-in-cell code [1] and the MCNP electron-photon Monte Carlo transport code [2] are linked statically using files that contain the data needed by each code. Beam propagation to the bremsstrahlung converter target is simulated using Merlin to include plasma and electromagnetic effects. The MCNP Monte Carlo code then models electron transport and photon generation in the target and interrogation of the object by the photons. We have used this capability to generate synthetic radiographs of the French test object (FTO), which are further analyzed to obtain material interface locations and density profiles. The integrated simulation capability allows us to vary all beam parameters and examine their effects on radiographic fidelity [3].

In our study, we assumed a typical radiographic electron beam of 20 MeV and 2 kA current is incident on a 1-mm thick tantalum foil. We found that the beam spot size is an important factor in determining spatial resolution of the reconstructed object; however, the angular distribution of the electron beam has minimal effect on fidelity. An increase in the spot size causes a proportional increase in the uncertainty of material boundary location. Our study also indicated that the energy dependence of photon mass attenuation requires that the photon energy spectrum must be taken into account in the reconstruction process to quantitatively determine material density.

II. Particle-in-cell (PIC) Simulation

There has been extensive research on the interaction of the electron beam with the converter target, and various methods have been proposed to achieve a stable minimum electron beam spot at the target surface [3]. In the final focusing region where the electron beam is focused down to 2-mm in diameter at the converter target, the electron beam dynamics must be treated self-consistently including all electromagnetic effects. Particle-in-cell simulation is appropriate in this regime because it couples the equation of motion governing individual charged particles and the full Maxwell's equations with appropriate boundary conditions in a finite-difference time-domain (FDTD) scheme. The two-dimensional (r-z) relativistic and fully electromagnetic code Merlin [1] is used to model the beam dynamics. In our simulation, we chose to place a gas cell of nitrogen with a pressure of 10 Torrs in front of the target with a pre-ionized plasma density of $1x10^{15}$/cc**,** which simulates impact ionization by the electron beam. The 20 MeV electron beam is injected from the left boundary into the gas cell of 2.0-cm axial length. The electron beam has a Gaussian velocity spread of 1%. The plasma in the gas cell has

a thermal energy spread of 2 eV. The electron beam is given a convergent angle as required to produce a 2-mm or 4-mm spot diameter at the target surface. We have performed three simulations with different beam and plasma conditions. The first simulation is a reference case in which the electron beam is ballistically focused onto the target with a spot size of 2-mm in diameter, ignoring all electromagnetic effects. This idealized simulation is used as a benchmark for comparisons. The second simulation allows the electron beam to propagate through the background plasma and also generates a spot size of 2-mm at the target. In the third simulation, we increase the spot size to 4-mm to examine the effect on the reconstructed object.

In Fig. 2, we show the simulation results from the case for the 2-mm spot size going though the 2-cm gas cell. The electron-neutral collisions are included using a treatment based on Moliere and Bethe formulation [1,4]. Electrons are continuously injected from the left boundary, and they are absorbed at the right boundary which corresponds to the target. The radial positions and momenta of the electrons reaching the right boundary are recorded in a data file, which then provides the electron source for the subsequent Monte Carlo electron-photon simulation. The electron beam takes about 0.067 ns to traverse the gas cell, and has a rise time of 0.033 ns to reach its full current of 2.0 kA. Figure 2 displays the electron beam "z - r" configuration space and "p_z/mc– z" phase space at a time of 0.5 ns. Growth of the plasma two-stream instability causes modulation of the beam radius and momentum [5]. With a choice the 2-cm gas cell, the convective instability is still in its linear phase when it reaches the target. Consequently, the perturbation is relatively small and does not significantly increase the beam spot size.

In Fig. 3, we show the characteristic time-averaged radial density profiles of the electron beam at the target for the three cases as obtained from our PIC simulations. In case 1, the beam density is lowest at the center and increases monotonically with radius. This effect is caused by the ballistic convergence angle. The localized radial variations in cases 2 and 3 reflect the spatial modulations due to the beam-plasma instability. Similarly, the angular distributions of the electron beam at the target surface are shown in Fig. 4. The radial convergence of the electron beam is responsible for the predominantly negative angular distribution. The positive angles are due to a slight amount of over focusing of the electron beam resulting in some electron crossings of the z-axis in front of the target.

III. Numerical Synthetic Radiographs and Tomographic Reconstruction

The data file containing the physical characteristics of the electron beam at the target is used as the source for the subsequent Monte Carlo calculations. In these calculations, the French Test Object (FTO) is placed 1-meter from the tantalum converter target and the detector is 1-meter behind the object (Fig.1). This setup has a magnification factor 2 from the radiographic object to the detector. The FTO consists of a set of concentric spheres with a void region at the center. The void has a radius of 1.0 cm, and the second and third layers are tungsten and copper with radii of 4.5 cm and 6.5 cm, respectively. The Monte Carlo code MCNP [2] is used to simulate propagation of the electron beam through the bremsstrahlung converter target and transport of the resulting photons through the FTO. The detector diagnostics in the calculations can give separate tallies of the radial distributions of the primary and scattered photons. Because of photon attenuation in different materials of the radiographic object, the radial distribution of the primary photons at the detector can become a radiograph when it is properly normalized

with the incoming photon flux. In Fig. 5a, we show the one-dimensional radiographs at the equator of the FTO generated by the linked computer simulations of the three cases. Due to the magnification factor, the material edge locations on the synthetic radiograph are expected to be at ±2.0 cm, ±9.0 cm, and ±13.0 cm. It is evident from Fig. 5a that excellent agreement has been obtained. Furthermore, the close identity of the three radiographs from the simulations indicates that the variations in the physical characteristics of the electron beam as shown in Figs. 3 and 4 do not affect the radiographic images significantly. To examine the effect of electron beam spot size, we show in Fig. 5b the region around the copper and tungsten interface at an expanded scale. The edge location is more blurred (lower spatial resolution) for the case with a 4-mm electron beam spot size. This points to the conclusion that the spot size is an important factor in the determination of spatial resolution.

Tomographic reconstruction was further applied to the synthetic radiographs to extract material boundaries and attenuation coefficients for each shell. A variety of algorithms were considered, but the principal technique used was Abel inversion. The reconstruction procedure is basically model independent and calculates the attenuation for each part of the object from the integral pathlength (attenuation x length) measured at each projection pixel. In this method, the object is modeled as a series of concentric rings of constant attenuation, where the cross-section of each ring is equal to the height and width of a single pixel on the projection array. Thus, in general, the edges of the circular rings will not correspond to the material boundaries. The object is reconstructed from the outermost ring to the center. For the outermost pixel, all the pathlength contribution will be determined by only the outer ring. The unknowns are attenuation and length of a

chord between the source and projection pixel that passes through the outer ring. But the chord length is given by geometry (a function of the radius from object center to ring), so the attenuation for the first ring can be calculated directly by dividing pathlength by chord length. For the next inward ring, the pathlength is given by contributions from the first (outermost) and second rings. Both chord lengths are again given by geometry, and the attenuation for the first ring is known, so the only unknown is attenuation for the second ring. The process is repeated until all rings have been reconstructed. The geometry portion of the problem can be represented as a matrix, allowing the attenuation to be solved by inversion.

The reconstruction of the FTO radiograph obtained from case 2 is shown in Fig. 6, which clearly indicates the object is composed of a void region in the center and two concentric layers of different materials. Furthermore, the material boundaries and relative attenuation coefficients are clearly identified. The horizontal axis is pixel number and the vertical axis is the relative absorption coefficient. The edge overshoots and the slight curvatures in a single material region are attributed to photon spectral effects on material mass attenuation. The current reconstruction algorithm does not include attenuation variations resulting from spectral effects, although iterative algorithms are being considered to address this issue. Spatial resolution of the tungsten/copper interface for the 2-mm and 4-mm spot sizes are compared in Fig. 7, illustrating the inverse relationship between spot size and resolution.

IV. Discussion

The capability of integrated system simulation in radiography has been demonstrated in the evaluation of the effects and sensitivities of physical parameters on radiographic

fidelity. The simulation tool has been applied to static radiography of the French Test Object. We found that the radiographic process is rather insensitive to angular spread of the electron beam. However, our study confirms that the beam spot size is a crucial parameter in resolution of spatial features. The spectral effects on tomographic reconstruction are currently being studied to determine material densities.

Acknowledgments:

The authors wish to thank Drs. K. L. Buescher, F. T. Cochran, B. G. DeVolder, and D. C. Wolkerstorfer for many useful discussions. This worked is supported by US DOE.

References

[1] Thomas J. T. Kwan and Charles M. Snell, "Methods of Monte Carlo Electron Transport in Particle-in-cell Codes," Lecture Notes in Physics, in Monte Carlo Methods and Applications in Neutronics, Photonics and Statistical Physics, edited by R. Alcouffe, R. Dautray, A. Forster, G. Ledanois, and B. Mercier (Springer, New York 1985).

[2] J. F. Briesmeister, et al., "MCNP – A General Monte Carlo Particle Transport Code, Version 4B," Los Alamos National Laboratory Report LA-12625-M, vers. 4B (1997).

[3] Thomas J. T. Kwan, Charles M. Snell, and Peggy J. Christenson, "Electron beam-target interaction and spot size stabilization in flash x-ray radiography," Physics of Plasmas, Vol. 7, No. 5, pp.2215-2223 (2000). Also references therein.

[4] H. J. Bethe and J. Ashkin, Experimental Physics, Vol. 1, E. Segre (ed.) John Wiley and Company, New York (1953).

[5] L. E. Thode, "Plasma heating by scattered relativistic electron beams: correlations among experiment, simulation, and theory," Phys. Fluids 19, 831 (1976).

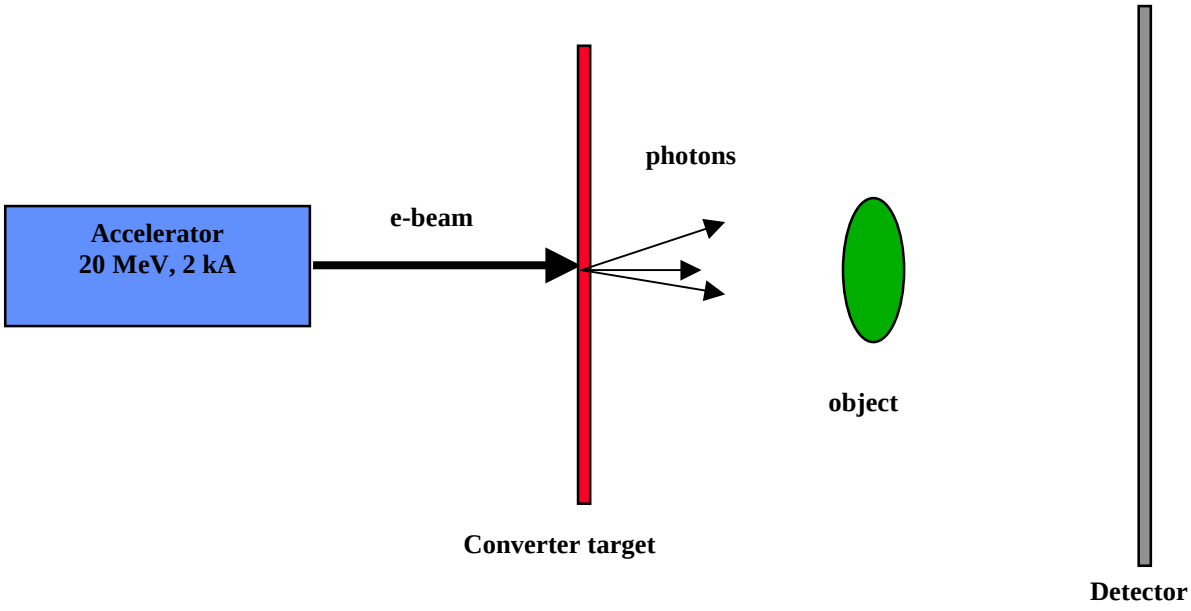

Fig. 1: Schematic of x-ray radiographic process

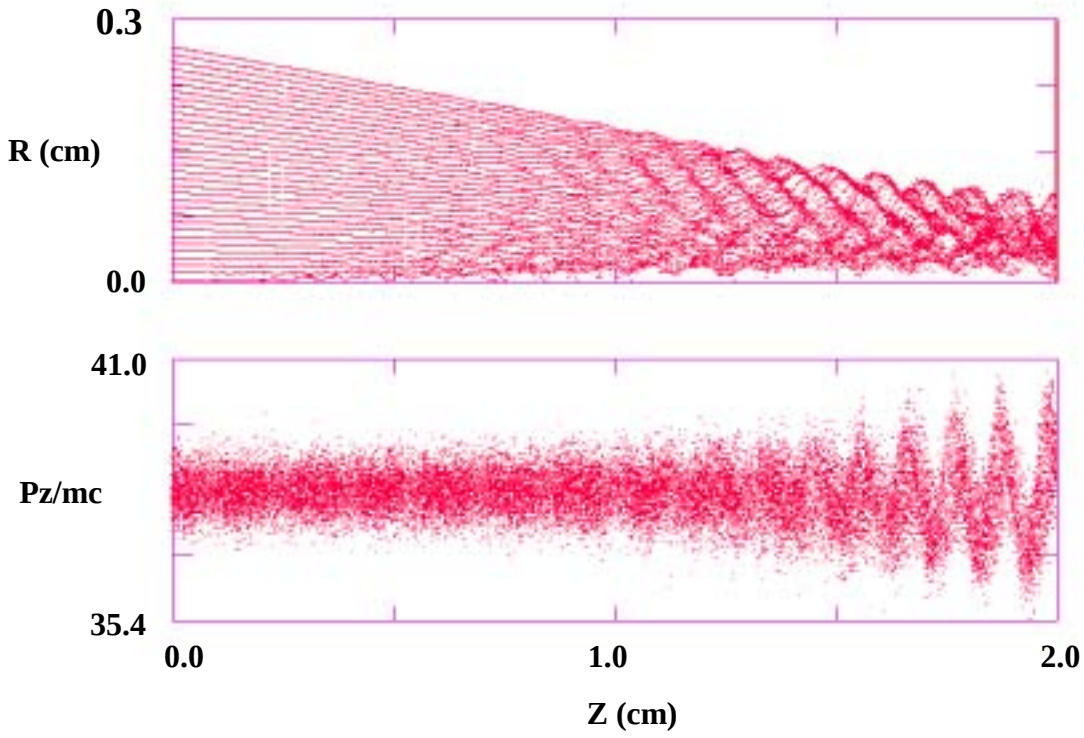

Fig. 2: The electron beam is focused onto the target (upper panel) while its interaction with the plasma in the gas cell leads to modulation in its phase space (lower panel).

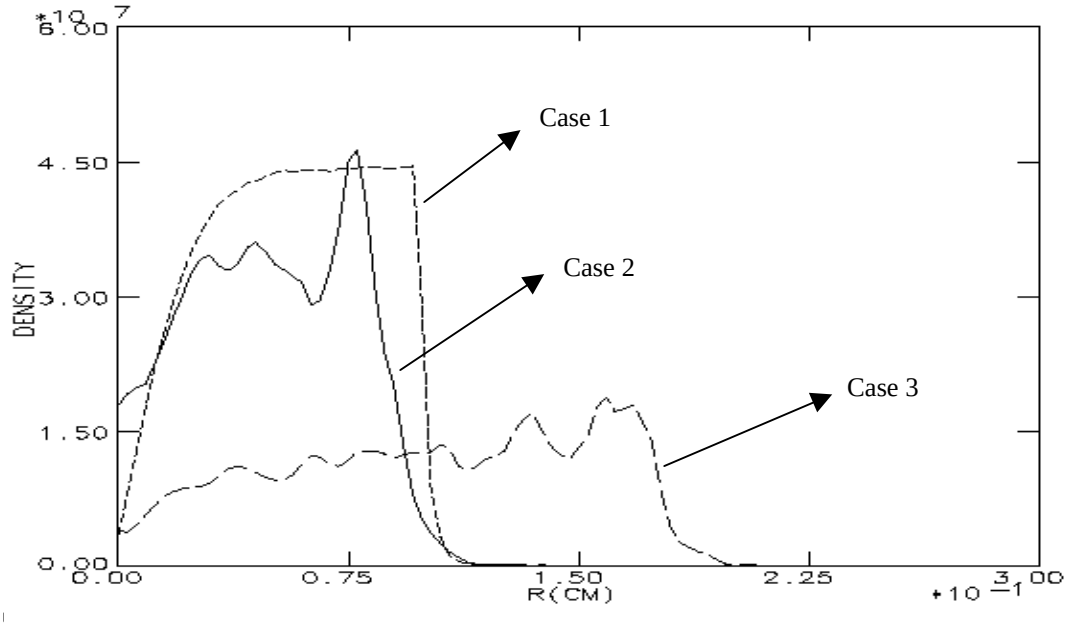

Fig. 3: Characteristic time-averaged radial density profiles of the electron beam at the target from PIC simulations. Vertical axis is arbitrary. Case (1): ballistically focused beam, electromagnetic effects ignored. Case (2): full electromagnetic simulation, 2-mm beam spot diameter. Case (3): full electromagnetic simulation, 4-mm beam spot diameter.

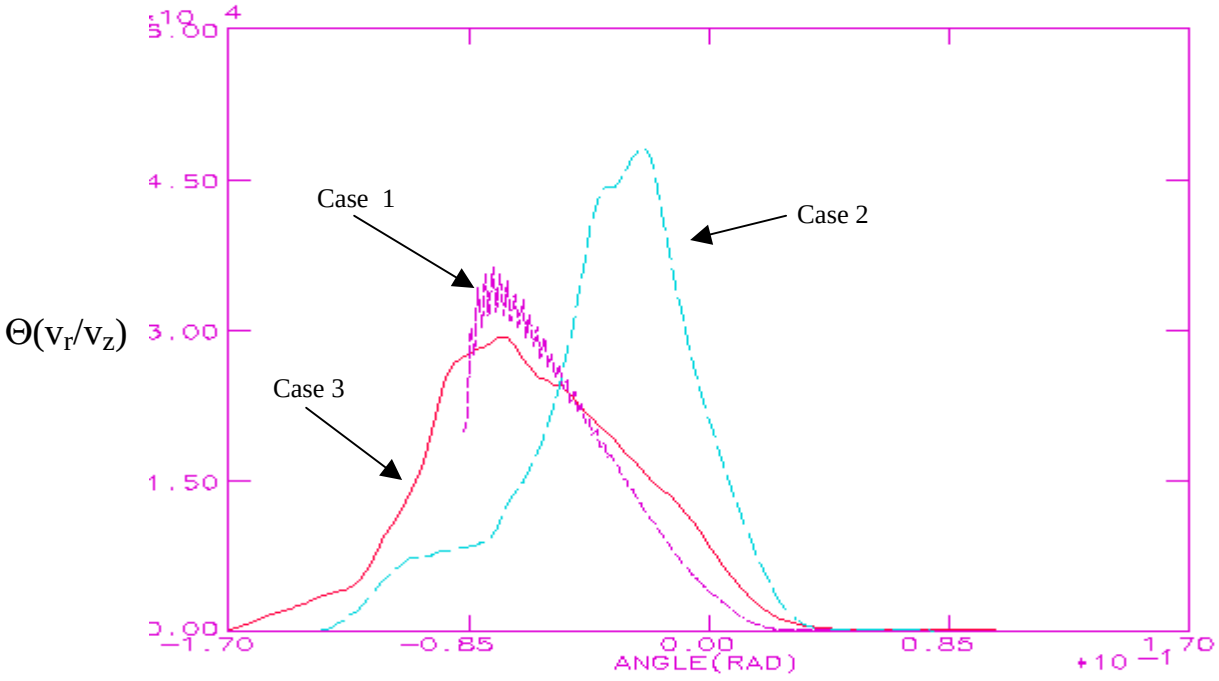

Fig. 4: Angular distributions of the electron beam from PIC simulations. Vertical scale is arbitrary.

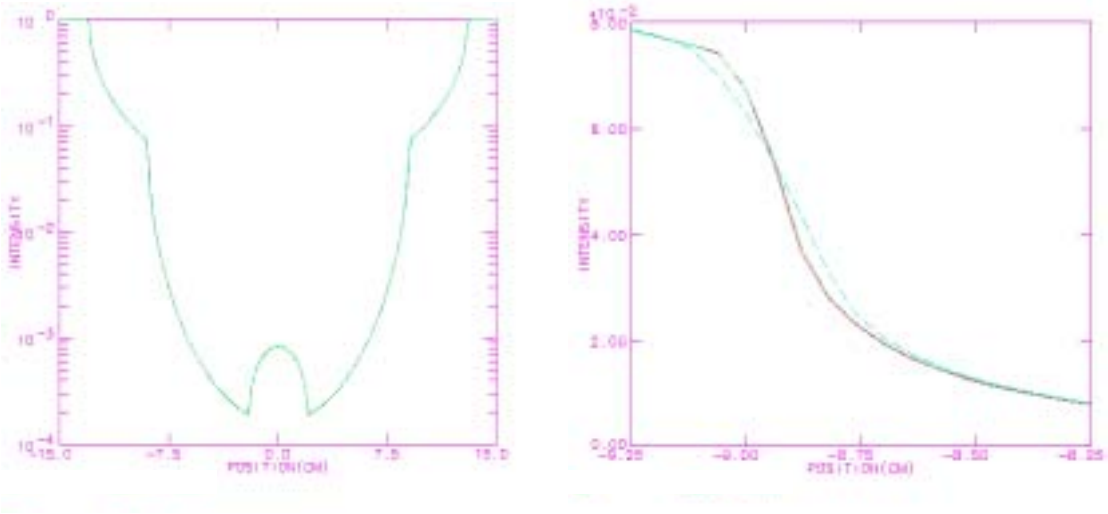

Figs. 5a & 5b: Synthetic radiographs obtained from the integrated simulation for the three electron beam cases (see text).

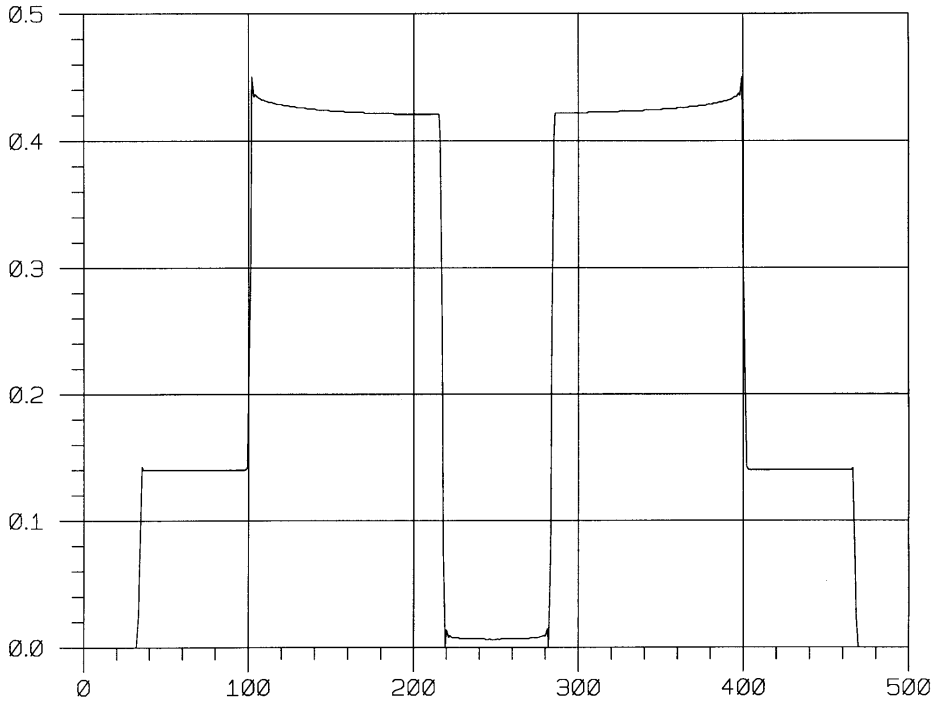

Fig.6: Image reconstruction of the radiograph obtained from the simulation of case 2.

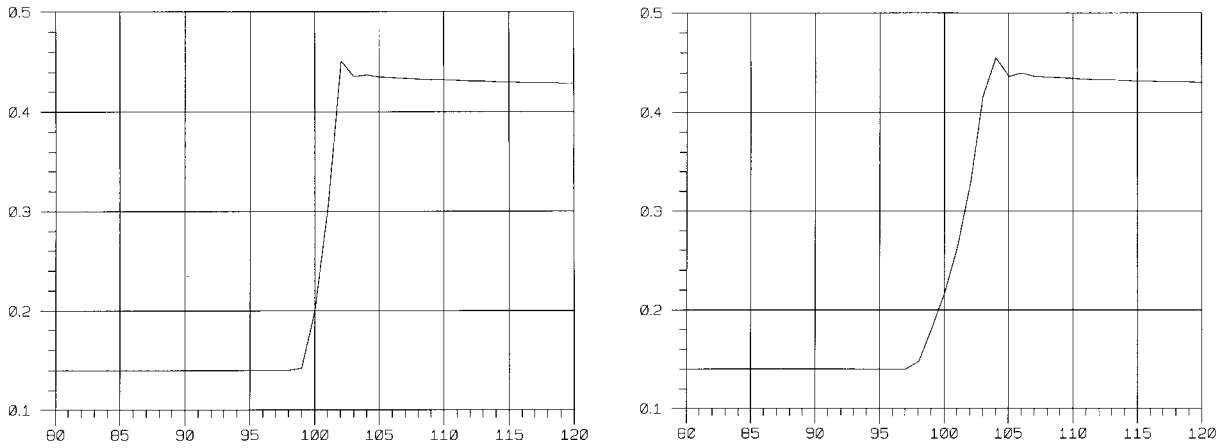

Fig.7: Edge location from image reconstructions from simulations of cases 2 (left panel) and case 3 (right panel).